Linköping Studies in Science and Technology
Thesis No. 1262

Multidimensional MRI of Cardiac Motion

Acquisition, Reconstruction and Visualization

Andreas Sigfridsson

Linköping University

LIU-TEK-LIC-2006:43

Department of Biomedical Engineering
Department of Medicine and Care
Linköping University, SE-581 85 Linköping, Sweden

Linköping, June 2006

Cover:
Left ventricular volume measured for all combinations
of cardiac and respiratory phases (from Paper II).

Multidimensional MRI of Cardiac Motion
Acquisition, Reconstruction and Visualization

Department of Biomedical Engineering
Department of Medicine and Care
Linköping University
SE-581 85 Linköping
Sweden

ISBN 91-85523-37-2 ISSN 0280-7971

Printed by LiU-Tryck, Sweden

Abstract

Methods for measuring deformation and motion of the human heart *in-vivo* are crucial in the assessment of cardiac function. Applications ranging from basic physiological research, through early detection of disease to follow-up studies, all benefit from improved methods of measuring the dynamics of the heart. This thesis presents new methods for acquisition, reconstruction and visualization of cardiac motion and deformation, based on magnetic resonance imaging.

Local heart wall deformation can be quantified in a strain rate tensor field. This tensor field describes the local deformation excluding rigid body translation and rotation. The drawback of studying this tensor-valued quantity, as opposed to a velocity vector field, is the high dimensionality of the tensor. The problem of visualizing the tensor field is approached by combining a local visualization that displays all degrees of freedom for a single tensor with an overview visualization using a scalar field representation of the complete tensor field. The scalar field is obtained by iterated adaptive filtering of a noise field.

Several methods for synchronizing the magnetic resonance imaging acquisition to the heart beat have previously been used to resolve individual heart phases from multiple cardiac cycles. In the present work, one of these techniques is extended to resolve two temporal dimensions simultaneously, the cardiac cycle and the respiratory cycle. This is combined with volumetric imaging to produce a five-dimensional data set. Furthermore, the acquisition order is optimized in order to reduce eddy current artifacts.

The five-dimensional acquisition either requires very long scan times or can only provide low spatiotemporal resolution. A method that exploits the variation in temporal bandwidth over the imaging volume, k-t BLAST, is described and extended to two simultaneous temporal dimensions. The new method, k-t^2 BLAST, allows simultaneous reduction of scan time and improvement of spatial resolution.

Acknowledgments

I would like to thank my supervisors, Hans Knutsson, Lars Wigström and John-Peder Escobar Kvitting. Hans provided me with a constant stream of ideas and broadened my vision. Lars introduced me to this field and taught me everything about magnetic resonance imaging. John-Peder guided me in understanding the function of the heart. Thank you for believing in me and giving me the encouragement I needed.

I would also like to thank my colleagues at the divisions of clinical physiology and medical informatics, the MRI unit and the Center for Medical Image science and Visualization (CMIV). You provided me with the atmosphere that I love and the opportunities for interesting discussions on a wide flora of topics. Thank you Tino, Einar, Jan, Ann, Eva, Carljohan, Per, Henrik, Petter, Marcel, Frida, Peter, Olof, Mattias, Johanna, Anders, Andreas, Björn, Joakim, Mats, Magnus, Pernilla, Katarina and Matts.

I would also like to take this opportunity to express my gratitude to the late Bengt Wranne for providing this environment and opportunity for me and many of my colleagues.

This work has been conducted in collaboration with the Center for Medical Image Science and Visualization (CMIV, http://www.cmiv.liu.se/) at Linköping University, Sweden. CMIV is acknowledged for provision of financial support and access to leading edge research infrastructure. This work was further funded by the Swedish Research Council, the Heart Lung Foundation and the Linköping Heart foundation.

Contents

Chapter 1

Introduction

Cardiovascular disease is the leading cause of death in the western world. In Sweden, diseases of the circulatory system was the cause of death of 45% of the men and 44% of the women who died in 2003 [1]. Of these deaths, ischemic heart disease was the largest group, accounting for 23% of male deaths and 18% of female deaths. Decades of research has been conducted to understand the function of the healthy heart, the changes associated with disease, and the causes thereof. Functional studies of the heart wall are the cornerstone for the assessment and follow-up of a large range of cardiac diseases. Cardiac motion and deformation are fundamental properties that are of interest to comprehend the impact of diseases on cardiac function. Quantification of motion and deformation would lead to less subjective assessment and improve our ability to compare the effect of different treatment strategies.

The aim of this thesis was to develop methods for measuring deformation and motion of the heart *in-vivo* with the use of magnetic resonance imaging (MRI).

To fulfill this goal, the following approaches were investigated:

- Visualization of the local heart wall deformation. This involves computing a strain rate tensor field from a volumetric velocity measurement of the heart. The strain rate tensor is insensitive to regional translation but instead describes the rate of local lengthening or shortening. The tensor field is visualized using a combination of traditional glyph rendering of a single tensor with tensor-guided adaptive filtering of noise fields for overview visualization.

- Acquisition of volumetric images resolved over both cardiac and respiratory cycles simultaneously. This produces a five-dimensional data

set, allowing for example measurement of interventricular coupling during the respiratory cycle. This is accomplished by combining a fast MRI pulse sequence with a triggering method extended to two simultaneous temporal dimensions. The acquisition order is optimized to minimize artifacts in the images.

- Acquisition time reduction by sampling data sparsely and exploiting spatiotemporal correlations during reconstruction. With this technique, the long acquisition time for five-dimensional imaging can be cut in half while spatial resolution is simultaneously quadrupled. The sparse sampling enables sharing temporal bandwidth between static and dynamic parts of the imaging volume, allowing for a significantly more efficient use of scan time.

1.1 Outline of the thesis

This thesis is organized as follows. In Chapter 2, a brief overview of motion of the heart during the cardiac and respiratory cycles is provided. Furthermore, the strain rate tensor, describing the local heart wall deformation, is introduced. Principles of cardiac MRI and temporally resolving sampling procedures in particular are presented in Chapter 3. In Chapter 4, ways to shorten acquisition time are discussed, mainly focused on the k-t BLAST method. Visualization of the heart wall deformation strain rate tensor field is described in Chapter 5. Chapter 6 contains short summaries of the papers that are part of this thesis, and Chapter 7 contains discussion.

1.2 Glossary of terms and abbreviations

Aliasing	The replication of a signal caused by periodic sampling. The aliased signal appears at different positions in the corresponding transform space, e.g. at different spatial positions, spatial frequencies, temporal positions or temporal frequencies.
ECG	Electrocardiogram
FOV	Field of view
In-vivo	Within a living organism, as opposed to in-vitro (in the laboratory).
k-space	The spatial frequency domain of the object being imaged in magnetic resonance imaging.
k-t BLAST	k-t Broad-use Linear Acquisition Speed-up Technique. A method to reduce acquisition time by sparse sampling in k-t space, with subsequent alias suppression during reconstruction.
LIC	Line integral convolution, a vector field visualization technique.
M-mode	Motion mode. Display of dynamics by presenting the temporal dimension on a spatial axis, widely used in ultrasound.
MRI	Magnetic resonance imaging
Myocardium	Heart muscle
SSFP	Steady State Free Precession. An MRI pulse sequence widely used for cardiac imaging.
TRIADS	Time-Resolved Imaging with Automatic Data Segmentation. A method for resolving motion with automatic division of the cycle into multiple time frames.
Voxel	Volume element

Chapter 2

Cardiac motion

There are several types, or scales, of cardiac motion that are meaningful to study. Deformation or strain in the cardiac muscle can give useful information about the local function of the muscle. Wall thickening and motion can also give important regional information. The interaction between the left and right ventricles is a more global effect that is influenced by pressure differences external to the heart, such as caused by respiration.

2.1 The cardiac cycle

The heart is the organ responsible for pumping blood throughout the body. It is divided into four chambers; the left and right atria and the left and right ventricles, as shown in Figure 2.1. The pump function of the heart is periodic, and the cardiac cycle is divided into two main phases, diastole and systole. In the diastolic phase, the left and right ventricles are filled with blood from the atria through the mitral and tricuspid valves. In the systolic phase, the ventricles contract and blood is ejected through the aortic and pulmonary valves to the aorta and the pulmonary artery.

Both the left and right sides of the heart beat approximately simultaneously. The two sides are connected in series with the systemic circuit through the body and the pulmonary circuit through the lungs. Deoxygenated blood from the body is delivered to the right atrium. The blood fills the right ventricle and is subsequently ejected through the pulmonary artery and into the lungs, where it is oxygenated. Oxygenated blood is delivered to the left atrium which then fills the left ventricle. The left ventricle ejects the oxygenated blood through the aortic valve to the aorta, which is connected to the rest of the body.

Common heart rates in healthy persons are 45–80 beats per minute.

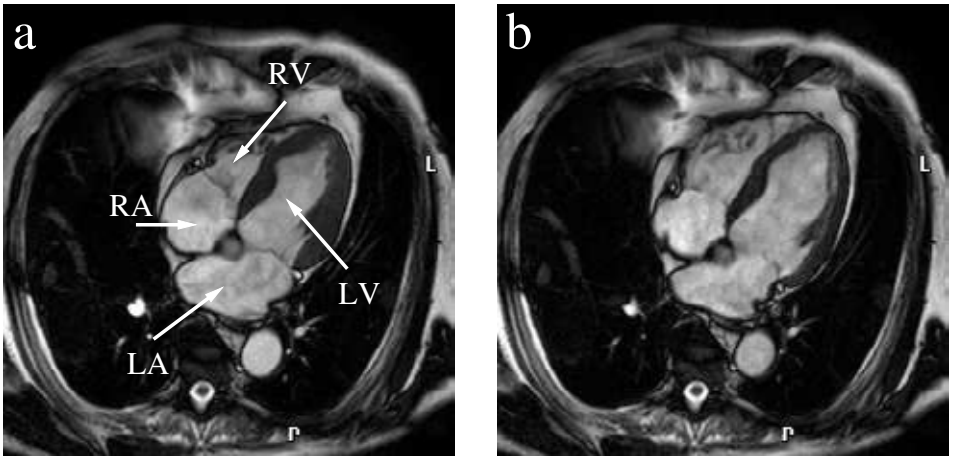

Figure 2.1: Cardiac configuration in systole (a) and diastole (b) in a four-chamber view. The arrows indicate the right ventricle (RV), right atrium (RA), left ventricle (LV) and left atrium (LA).

The duration of the systolic phase usually varies very little with changing heart rates, but the duration of the diastolic phase can vary substantially. The thickness of the myocardium, the heart wall, of the left ventricle ranges from around 10 mm at the end of diastole to 15 mm at the end of systole. The right ventricular walls are significantly thinner, measuring 5.3 mm and 5.6 mm in end diastole and end systole, respectively. The outer contours of the heart are surprisingly static during the cardiac cycle, as shown in Figure 2.1. Substantial contribution to the volume changes is made by shifting the atrio-ventricular plane in the apex to base direction with the valves open during diastole and in the opposite direction with the valves closed during systole [2].

What is commonly measured to assess cardiac motion is wall thickness variations during systole and diastole. Synchrony of the different parts of the ventricle can also be of interest, especially when studying effects of myocardial ischemia and infarction [3].

2.2 The respiratory cycle

Cardiac motion is highly affected by respiration. The most dominant effect of respiration is the effect on heart position. During inspiration, the diaphragm, a muscular interface between the abdominal and thoracic cavities, pulls downward, allowing the lungs to expand. The heart is attached to the diaphragm, and is being pulled down during inspiration. Chest muscles

also expand the chest cage, but to a much lesser extent than the expansion caused by the diaphragm. This is illustrated in Figure 2.2.

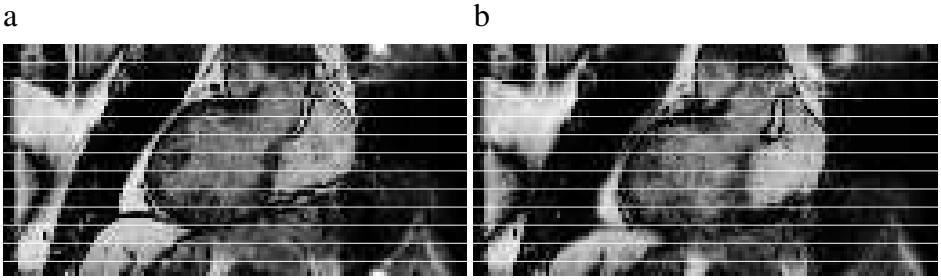

Figure 2.2: Cardiac positions in end expiration (a) and end inspiration (b). The heart is shifted as the diaphragm is pulled down during inspiration.

Respiration also affects the pressure in the thorax. During inspiration, pressure is lowered, to force air from the outside into the lungs. This lowering of pressure reduces resistance in the vena cavas, the veins that transport deoxygenated blood from the body into the right atrium. This in turn increases filling of the right ventricle. At the same time, resistance in the pulmonary system is increased, *reducing* the filling of the left ventricle. During expiration, the pressure and the corresponding effects are reversed.

Typical respiratory rates vary between 10–20 cycles per minute. The heart can be shifted as much as 12 mm. The effects of respiration is more individual than that of the cardiac cycle.

2.2.1 Interventricular coupling

With changing pressures in the thorax, filling of the ventricles is affected differently in the left and right sides. This results in changing volumes and pressures between the ventricles. The interventricular septum regulates this, shifting from one side to the other, in order to allow for volume or pressure increase. This shift has been demonstrated by the method presented in Paper II and is shown in Figure 2.3. This is referred to as coupling between the ventricles, and is important in several diseases. Some diseases affect the pericardium surrounding the heart. A stiffer pericardium will exaggerate the interventricular coupling. The ventricular coupling is present even without any pericardium, but the effect is reduced [4]. Acute changes in left ventricular function due to abrupt pressure overload of the right ventricle (e.g., from pulmonary embolism) may be explained by interventricular coupling. Long-term right ventricular volume overload, for example caused by pulmonary valve insufficiency, can also be linked to the interventricular

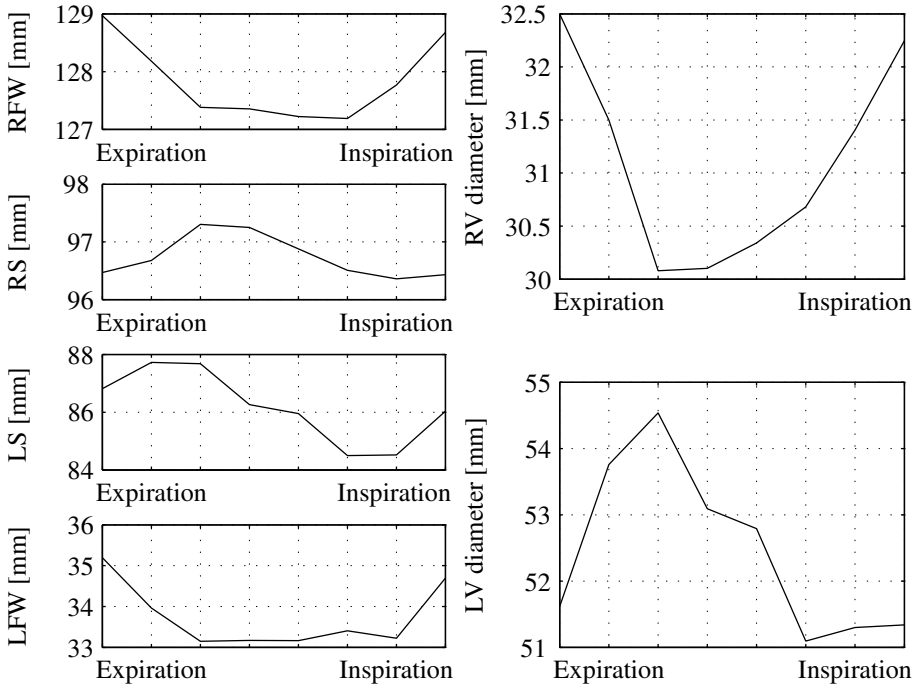

Figure 2.3: Septal motion over the cardiac cycle, presented in Paper II. The wall positions of the inner right ventricular free wall (RFW), right side of the septal wall (RS), left side of the septal wall (LS) and inner left ventricular free wall (LWF) were traced through the respiratory cycle in an end diastolic cardiac phase and shown on the left. Note that the septal wall moves towards the right ventricle during expiration and towards the left ventricle during inspiration. On the right, the computed right ventricular (RV) diameter and left ventricular (LV) diameter show RV diameter decreasing during expiration and increasing during inspiration. LV diameter demonstrates the opposite behavior.

interdependence [5]. After open heart surgery, abnormal septal wall motion is commonly observed [6]. The pathophysiological mechanism behind this phenomenon is still disputed [7, 8].

2.3 Myocardial deformation

Local deformation of the myocardium is an important measure of its function. In the deformation estimate, translation is usually excluded, providing only a measure of local lengthening and shortening. Damaged muscle tissue is expected to produce less deformation, but it may still show large

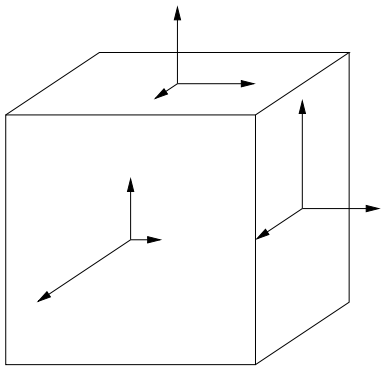

Figure 2.4: Illustration of the stress tensor acting on a point. The tensor components are the stresses acting on different cut planes.

translation, due to pulling or pushing by neighboring healthy tissue [2].

Deformation and stress of a small volume is usually quantified using a tensor. The general definition of a tensor involves a vector space V and its dual. We will only be interested in the case where V is equipped with a fixed scalar product, in which case the definition of a tensor is a multilinear mapping from a number of vector spaces (V) onto the real space ($\mathbf{R}$). The rank of a tensor is the number of arguments to the mapping. Scalars and vectors are special cases of tensors, namely tensors with ranks 0 and 1, respectively. We will consider the special case of tensors with rank 2. In this case, the tensor is a bilinear mapping $V \times V \to \mathbf{R}$. There is a one-to-one correspondence of these tensors with mappings $V \to V$. The tensor is then naturally identified with this latter mapping.

Internal forces acting on a body can be described by the stress tensor. One may think in terms of virtually cutting the body along a cut plane. There is a force acting upon this cut plane, not necessarily perpendicular to the plane, but generally having components of shear orthogonal to the plane normal. This is illustrated in Figure 2.4. The stresses acting on three orthogonal cut planes are shown on the surfaces of a box. The stresses can be of arbitrary direction, as illustrated by the decomposition into three orthogonal components, one in the normal direction, representing the normal stress, and two in the surface plane, representing shear stress. Since the tensor is linear, the stress vectors need only to be obtained for three linearly independent cut planes in order to determine the tensor completely.

The stress tensor is the linear mapping from the cut plane, which may be represented by its normal vector, to the stress vector. The correspondence with the mapping $V \times V \to \mathbf{R}$ is then how much stress on a cut plane (first

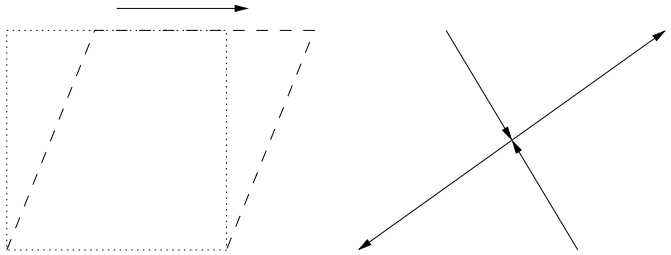

Figure 2.5: Eigen decomposition of the deformation of a square. The dotted square is the original state and the stippled parallelogram is the deformed state. The arrow on the square indicates shear force. The eigen decomposition is illustrated to the right, with a large lengthening in one diagonal direction and a somewhat smaller shortening in the other diagonal direction.

argument) there is along a probe vector (second argument).

Eigen decomposition is useful to aid interpretation, after which three (in three dimensions) eigenvectors and corresponding eigenvalues are obtained. The eigen decomposition is easiest considered when viewing the tensor as the mapping $V \rightarrow V$ and representing the cut plane with its normal vector. An eigenvector $\mathbf{e}$ to a mapping $\mathbf{T}$ is a vector which is mapped to itself scaled by the eigenvalue λ, i.e. $\mathbf{Te} = \lambda\mathbf{e}$ with $\mathbf{e} \in V$. In other words, the eigenvector is the normal to a cut plane containing only normal stress and no shear stress. An example of eigen decomposition is illustrated in Figure 2.5

Common notation for the stress tensor components is a 3×3 matrix. The Cauchy stress tensor is symmetric [9], so the matrix representation is also symmetric. This means that the eigenvalues are real and the eigenvectors are orthogonal.

With the stress tensor representing stress, force per unit area, there is a corresponding strain tensor, representing local normalized deformation. The strain tensor is related to the stress tensor through a constitutive law. Strain reflects the shape change between two states, one state usually being some kind of reference state. This usually requires tracking of points through time, not readily available with non-invasive methods such as MRI. Tagging [10] or point tracking in velocity fields [11] can provide data suitable for estimating myocardial strain, but limitations in spatial resolution makes this approach difficult. Another way to characterize myocardial deformation is to directly measure velocity by using phase contrast MRI [12, 13]. From the measured velocity field, a spatial derivative, the

Jacobian $\mathbf{L}$, can be computed according to

$$\mathbf{L} = \nabla \mathbf{v} = \frac{d\mathbf{v}}{d\mathbf{x}} \sim \begin{pmatrix} \frac{\partial v_1}{\partial x_1} & \frac{\partial v_1}{\partial x_2} & \frac{\partial v_1}{\partial x_3} \\ \frac{\partial v_2}{\partial x_1} & \frac{\partial v_2}{\partial x_2} & \frac{\partial v_2}{\partial x_3} \\ \frac{\partial v_3}{\partial x_1} & \frac{\partial v_3}{\partial x_2} & \frac{\partial v_3}{\partial x_3} \end{pmatrix} \tag{2.1}$$

where $\sim$ denotes component representation, $\mathbf{v} \sim (v_1\ v_2\ v_3)^T$ is the velocity vector and $\mathbf{x} \sim (x_1\ x_2\ x_3)^T$ are the spatial coordinates. The asymmetric part of the Jacobian represents the rigid body rotation, while the symmetric part is called the *strain rate tensor*. The Jacobian is symmetrized according to

$$\mathbf{D} = \frac{1}{2}(\mathbf{L} + \mathbf{L}^T) \tag{2.2}$$

This tensor represents the instantaneous rate of change of strain and has the physical unit s^{-1}. The strain rate tensor is commonly used in fluid studies, but may also be applied to studies of myocardial mechanics.

By studying the strain rate instead of the velocity, information is not contaminated by translation possibly caused by adjacent muscle contraction and relaxation. The price for this convenience is the necessity to study the higher dimensional quantity of the tensor instead of the much simpler vector valued velocity. This can be alleviated to some extent by performing eigen decomposition of the tensor. The directions of the eigenvectors represent the principal directions of lengthening or shortening. In the case of the strain rate tensor, the eigenvalue then represents the rate of lengthening (positive) or shortening (negative).

Chapter 3

Cardiac Magnetic Resonance Imaging

3.1 MRI Principles

MRI is an imaging modality that exploits the nuclear magnetic resonance phenomenon, and is commonly used to produce images of the hydrogen proton distribution in humans. Hydrogen is abundant in the human body in the form of water molecules. MRI incorporates a strong external homogeneous magnetic field, which is used to align the spin distribution of the hydrogen protons along the magnetic field direction. A rotating magnetic field, usually referred to as radio frequency field, is then applied. Tuned to the Larmor frequency of the spins, it is used to tip the spin distribution away from the main magnetic field direction. This tipping is referred to as excitation. After the excitation, the spin distribution undergoes a relaxation process, in which the distribution returns to be directed along the main magnetic field. During this relaxation, the spins emit a signal that is received using induction in coils. During signal reception, additional spatially varying magnetic fields, referred to as the gradients, are applied to encode the spatial position of the signal. The combination of gradient waveforms and rotating magnetic field pulses is called a pulse sequence.

3.2 k-space

In MRI, data is naturally acquired in the Fourier domain, which is called k-space. During readout of the MRI signal, which is usually seen as a complex-valued signal, the spatially varying gradients encode a linear phase on the imaging object. A gradient with strength G applied during a time

period of t modulates the signal at a location x according to

$$e^{ix\gamma \int_0^t G(\tau)\mathrm{d}\tau} \tag{3.1}$$

where γ is the gyromagnetic ratio of the hydrogen proton. Combined with the fact that the signal is received from the whole object simultaneously and the substitution $k = \frac{\gamma}{2\pi} \int_0^t G(\tau)\mathrm{d}\tau$, the signal S follows a familiar relationship, a Fourier transform:

$$S = \int_X \rho(x) e^{ix2\pi k} \mathrm{d}x \tag{3.2}$$

where the integral is performed over all spatial positions and ρ is the proton density. This is a highly simplified model, disregarding relaxation, signal decay and spatially varying coil sensitivity during reception, among other things. Nevertheless, it illustrates the Fourier encoding and the role of k-space as the spatial frequency domain.

The waveforms of the gradients are chosen in order to collect data from different parts of k-space. The sequence of excitation and signal reception during gradient application is repeated many times to collect signal from sufficient parts of k-space to be able to reconstruct an image of the object. Each repetition uses a different gradient strength for the spatial encoding, to sample different points in k-space. The gradients can be applied in any spatial direction, making it possible to acquire three-dimensional images. A special case is the so-called "read-out" or "frequency encoding" direction. The gradient in this direction is commonly applied constantly *during* the signal reception, making a sweep through k-space in this direction while the signal is sampled at a high sampling frequency. This is the measurement of a k-space line, sometimes referred to as a k-space profile.

For objects with sharp details, high spatial frequencies need to be sampled. This requires sampling of a larger area of k-space using several repetitions and, consequently, a longer acquisition time. Since the spatial frequency domain is being sampled instead of the normal spatial domain, function domain and transform domain can be seen as reversed when compared to conventional signal processing of temporally or spatially sampled signals. Concepts of sampling density and Nyquist aliasing etc. show up in new places. Since humans have a finite spatial extent, the sampled signal is guaranteed to be band limited. This translates into a requirement for the sampling density in k-space to be able to reconstruct the object without aliasing. If k-space is not sampled densely enough, *spatial* aliasing will occur. This is because regular sampling in the function domain (k-space) will cause periodic repetition of the signal in the reciprocal trans-

form domain (the spatial domain). The sampling can be represented as a multiplication by the shah-function, III(k), defined as[1]

$$\text{III}(k) = \sum_{n=-inf}^{inf} \delta(k-n) \tag{3.3}$$

with δ as the Dirac impulse. The convolution theorem states that multiplication of two signals in the function domain corresponds to convolution of their transforms in the transform domain. Since III(k) is self-reciprocal [14], i.e. it is its own Fourier transform, this means that the transform of the sampled signal is replicated, or aliased, periodically. Furthermore, the similarity theorem states that if a function $f(x)$ has the Fourier transform $F(s)$, then the Fourier transform of $f(ax)$ is $\frac{1}{|a|}F(\frac{s}{a})$. This means that the aliased signals get closer to each other with larger sampling distance. If the aliased signals overlap, the true signal can no longer be recovered correctly.

3.3 *k-t* sampling

In dynamic imaging, k-space must be sampled over time as well. Time is discretized in a number of time frames with sufficient rate to capture the dynamics of the object being imaged. The standard method is to sample each k-space position once in every time frame. This can be referred to as regular sampling of the k-t space with full density, shown in Figure 3.1 together with the resulting aliasing of the signal in the x-f space.

To reconstruct the data sampled with full density as above, a rectangle function can be used to cut out the transform of the main signal. If data is not fully sampled, or equivalently, if the transform is larger than expected, the aliased signals will overlap with the main signal transform, causing reconstruction errors, as shown in Figures 3.2. This is actually quite often the case, especially in the temporal dimension, because the object being imaged is seldom truly bandlimited in the temporal dimension. This is not a big problem, because the energy content in the high temporal frequency components is very small compared to in the lower frequency components.

3.4 Temporal resolution

Requirements for spatial and temporal resolution for cardiac imaging often require acquiring data over the course of several heart beats. By assuming

[1]The shah-function is usually defined as a function of x, but since sampling in MRI is performed in k-space, the argument variable k is used here.

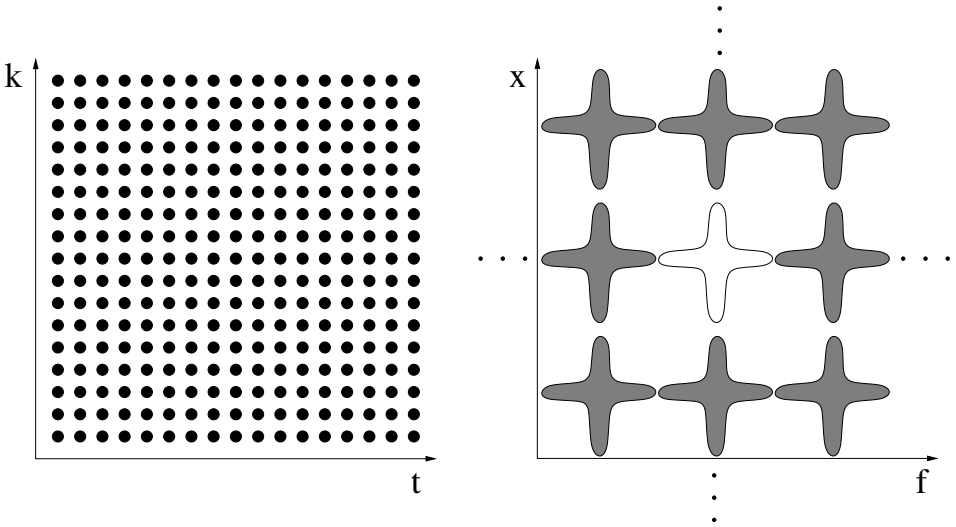

Figure 3.1: Regular k-t sampling with full density. Each dot shows a sampling position (left) and the corresponding transforms of the signal (right, white) and aliased signal (right, gray) are separated enough, enabling alias-free reconstruction.

that the object undergoes identical motion in each heart beat, different parts of k-space can be sampled in the same cardiac phase but in different cardiac cycles. This is a quite good approximation, but degraded by respiration or arrhythmia during the acquisition.

There are different methods of controlling k-space acquisition order and keeping track of which parts of k-space have been acquired during the experiment.

3.4.1 Prospective cardiac gating

Prospective cardiac gating [15], sometimes called triggering, works by alternating monitoring of a cardiac triggering device, such as an electrocardiogram (ECG), and acquisition of k-space data. The acquisition scheme starts by waiting for an R-peak in the ECG, meaning the onset of systole. After the R-peak is detected, the acquisition is delayed for a predetermined time, *trigger delay*. After the trigger delay, a fixed predetermined number of time frames are collected by acquiring another fixed predetermined number of k-space profiles for each time frame. After acquiring data from all time frames, monitoring of the triggering device is repeated. In each successive cardiac cycle, different lines in k-space are acquired. The acquisition is finished when all k-space lines have been acquired.

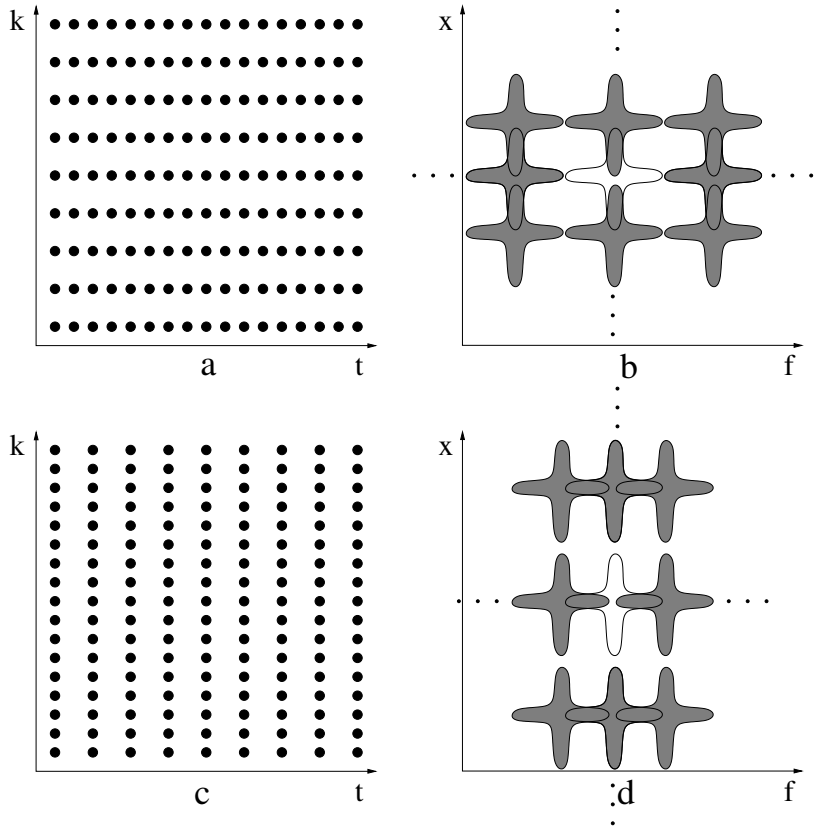

Figure 3.2: Regular k-t sampling with half density in the spatial frequency dimension (a) results in overlapping aliased signals (b), causing spatial aliasing errors after reconstruction. Regular k-t sampling with half density in the temporal dimension (c) also results in overlapping aliased signals (d), causing temporal frequency aliasing errors after reconstruction.

In prospective methods, the time frames are classified already during acquisition, making reconstruction easy. No interpolation is necessary and all cardiac cycles and k-space lines have the same number of time frames.

The drawback of this method is its inability to image the later parts of the cardiac cycle, because the number of cardiac time frames acquired needs to be fixed and set small enough to allow the scanner to start monitoring the ECG before the next R-peak. Some variation of cardiac frequency is expected, further limiting the number of cardiac time frames. The advantage is the simplicity of acquisition and reconstruction. This method is often used when only one time frame in a specific phase of the cardiac cycle is of interest, such as coronary artery magnetic resonance angiography.

3.4.2 Retrospective cardiac gating

Retrospective cardiac gating [16], often referred to as cine imaging, solves the problem of imaging the whole cardiac cycle. One common approach incorporates simultaneous acquisition and monitoring of the ECG. In the simplest form, acquisition starts by continuously measuring the first k-space line. When an R-peak is detected, acquisition is advanced to the next k-space line. Acquisition is terminated when the whole k-space has been acquired. Instead of only acquiring one k-space line continuously, one can alternate between several, trading temporal resolution for scan time. Also, k-space order is not necessarily linear from top to bottom, but can follow more advanced schemes.

Because of variations in heart rate, the number of measurements for each k-space line is not the same for every k-space line. The k-space data is then usually interpolated over time to a number of evenly distributed time frames. This interpolation usually stretches the cardiac cycle linearly, but some more advanced models have been proposed. One such model assumes a constant length systole and stretches diastole linearly, but it has not shown significant improvement over the simple linear model [16].

The benefits of the retrospective method is the ability to resolve the complete cardiac cycle, at the expense of implementation complexity.

3.4.3 TRIADS

A method that provides a flexible trade-off between acquisition time and temporal resolution is Time Resolved Imaging with Automatic Data Segmentation (TRIADS) [17]. Instead of following a fixed scheme for every cardiac cycle, acquisition is adapted to the cardiac phase. TRIADS decides which k-space line to acquire at a given time, in contrast to the cine method, which decides the time(s) to acquire a given k-space line. For every repetition of the TRIADS acquisition, the current cardiac phase is estimated. The estimated cardiac phase is then binned into one of a fixed number of time frames prescribed. TRIADS keeps track of which parts of k-space have already been acquired for each individual time frame, and acquires a new k-space line. The acquisition continues until a full k-space has been acquired for all time frames.

In cine imaging, temporal resolution is prescribed by a fixed multiple of the repetition time, which leads to varying number of time frames acquired for each k-space line. In contrast, TRIADS prescribes a number of time frames, and every cardiac cycle is divided into this number of time frames. Temporal resolution in milliseconds will then vary to be able to fit the

number of time frames into the cardiac cycle. A schematic comparison between the cine method and TRIADS is shown in Figure 3.3.

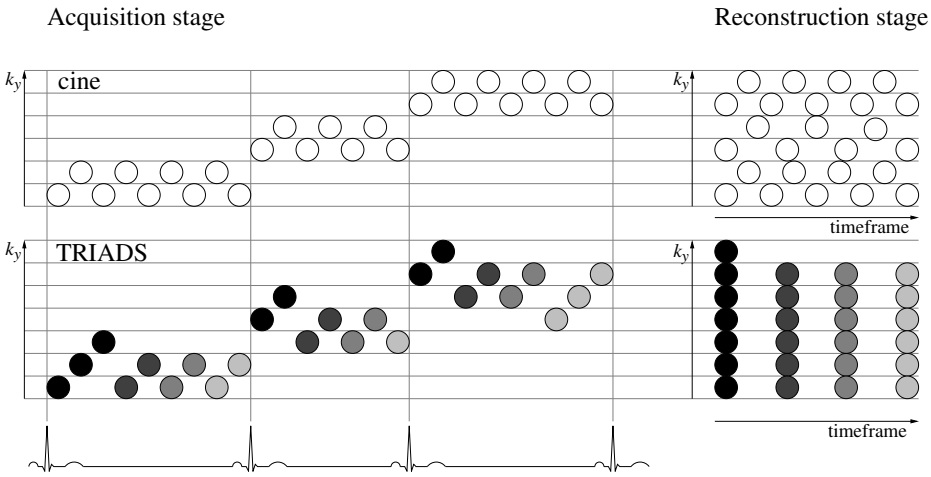

Figure 3.3: An example of cine and TRIADS acquisition schemes. In cine imaging, the acquired profiles (k_y) are changed at each R-peak. In TRIADS, cardiac phase, shown as circles with different shades in this example with four time frames, is estimated for each repetition. Previously acquired profiles are tracked individually for each time frame. Note that in TRIADS, the time frames are not required to come in a predictable order.

Since the binning into time frames is done during acquisition in TRIADS, reconstruction is as simple as for the prospective method. Indeed, one may regard TRIADS as a prospective method, as the binning into time frames usually involves predicting the duration of the current cardiac cycle based on previous cardiac cycles, as opposed to designating time retrospectively. A major difference between TRIADS and prospective gating is TRIADS ability to image the complete cardiac cycle. Retrospective re-binning may be performed by interpolation, refining the cardiac phase estimates. This requires that appropriate k-space lines have been acquired at a reasonable number of time points spread over the cardiac cycle. The prospective phase estimates thus still needs to be accurate to some extent.

3.4.4 Simultaneous resolution of both cardiac and respiratory cycles

In order to measure cardiac motion affected by respiration, the respiratory cycle needs to be resolved. Since there is still motion during the cardiac cycle, sampling must be synchronized with the cardiac cycle. This can

be accomplished by using a prospective triggering approach and acquiring only one time frame per cardiac cycle, but this reduces scan efficiency, because time is wasted waiting for the particular period in every cardiac cycle. Better efficiency can be achieved by continuously acquiring data, resolving both cardiac and respiratory cycles simultaneously. This means, acquiring a full image or volume for every combination of cardiac phase and respiratory phase. This adds a new dimension to cardiac imaging, being able to freeze motion during the cardiac cycle and examine what effects the respiration induces on cardiac function.

With simultaneous resolution of both cardiac and respiratory cycles, the time line becomes two-dimensional. If the cardiac and respiratory cycles are fully covered, as when using the TRIADS method, both dimensions are cyclic. The topology of the temporal dimensions can then be visualized as a torus, as shown in Figure 3.4. Even though the individual temporal dimensions are cyclic, their combination in actual time is more complex. This makes the cine and prospective methods unsuitable for acquiring data resolved to both dimensions simultaneously. The TRIADS method, however, only requires that the phases in the individual cycles can be estimated. Every repetition in the acquisition then involves estimating both cardiac and respiratory phase, classifying them into a combined time frame, and the TRIADS scheme takes care of filling the k-space in every time frame.

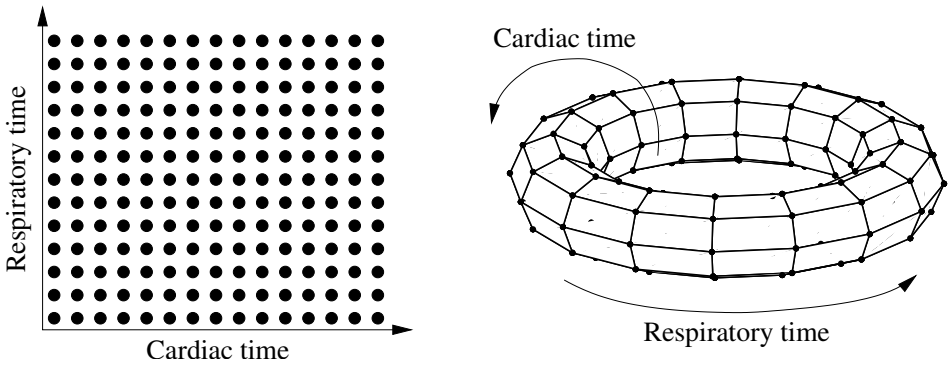

Figure 3.4: Simultaneous resolution of both cardiac and respiratory cycles gives a two-dimensional temporal plane (left). Since the plane is cyclic in both dimensions, the topology can be visualized as a torus (right).

Acquisition of simultaneous resolution of cardiac and respiratory cycles in a two-dimensional slice has been presented previously [18]. In that work, TRIADS was used to resolve the respiratory cycle, but within each cardiac cycle, retrospective cine imaging was performed. This caused the respiratory phase estimates made at the beginning of every cardiac cycle to be

assumed constant throughout that cardiac cycle. In Paper II, a volumetric method is presented, extending TRIADS to two simultaneous temporal dimensions.

3.5 k-space acquisition order

In cardiac imaging, balanced steady-state free precession (SSFP) [19] is a frequently used pulse sequence. It provides strong signal from the blood and allows for short repetition times with maintained signal level. This comes at the requirement of a fast gradient switching system and a stable homogeneous magnetic field. Gradient systems that are fast enough are readily available, but disturbances in the magnetic field can in some cases be a problem. One cause of problem is eddy currents disrupting the steady state. These eddy currents can be caused by large changes in phase encoding gradient strength between successive excitations [20], i.e. large jumps in k-space.

These effects can be removed by acquiring the same k-space line twice in two successive excitations and taking the complex average [21]. This will double acquisition time, however. A way to reduce the effects is to minimize the jumps in k-space by choosing an appropriate acquisition order. For prospective and retrospectively gated acquisitions, this is easy, since the k-space order can be controlled directly, and jumps can be minimized by choosing a zig-zag pattern. In TRIADS, however, the already acquired parts of k-space are generally different for different time frames. Time frames may be acquired in a non-predictable order, especially when resolving two independent temporal dimensions. Furthermore, the time between excitations is very short, imposing a limit to how much computations can be performed in order to optimize the acquisition order in runtime. In Paper II, this is solved by using a predefined k-space profile order curve and keeping a time-frame local progress counter that indicates how many lines along this profile order curve have been acquired for that particular time frame. The profile order curve is a discrete mapping from the one-dimensional progress counter to the two-dimensional $k_y - k_z$ space. The k_x dimension is covered by reading a whole line in k-space for each repetition. Typically, the time spent in each time frame is on the order of 10–15 excitations until the time frame is changed. Since all timeframes are approximately equally common, the differences between progress counters is expected to be small. This imposes three design criteria on the profile order curve:

- Each point in the $k_y - k_z$ plane should be visited exactly once.

- Two subsequent points along the curve should be adjacent to each other in $k_y - k_z$ space.
- The distance in $k_y - k_z$ space between two fairly close points on the curve should be minimized.

A curve which addresses these design goals is the Hilbert curve, proposed by David Hilbert in 1891. The locality of the Hilbert curve is close to optimal [22], meaning the maximum value of

$$\frac{|Hilbert(p_1) - Hilbert(p_2)|^2}{|p_1 - p_2|} \tag{3.4}$$

has a low bound. The squared distance in the numerator is computed in $k_y - k_z$ space and the distance in the denominator is the distance along the curve for two different points p_1 and p_2. This means that close points along the curve are also close in the $k_y - k_z$ space. Thus, when the time frame differs between excitations, the jump in k-space will be kept short. A first order Hilbert curve consists of a single U-shape as seen in Figure 3.5a. Subsequent levels are generated by replacing the U-shape with four rotated versions linked together with three joints (Figure 3.5b-d).

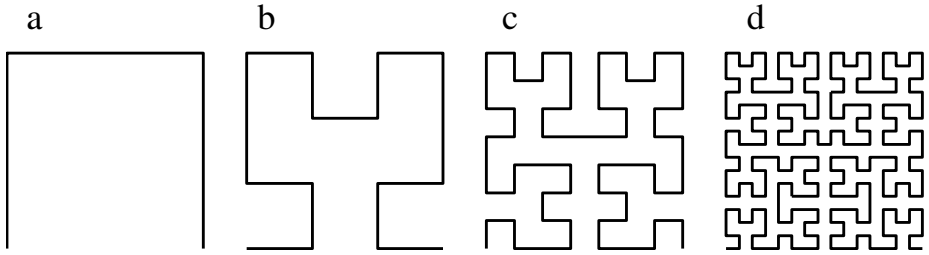

Figure 3.5: A Hilbert plane filling curve can be used to control acquisition order to reduce eddy current effects in balanced SSFP imaging. It is constructed recursively, and levels 1 through 4 are shown in a-d.

Chapter 4

Rapid acquisition

The demands for spatial and temporal resolution in cardiac MRI are usually not compatible with the desired acquisition time. Spatial resolution may be improved by acquiring more of k-space, at the expense of increased scan time and decreased signal-to-noise. Scan time may be reduced by decreasing temporal resolution, which is often not desirable. Increase of temporal resolution is also usually limited by the shortest repetition time available. Much effort has been put into reducing scan times while maintaining spatiotemporal resolution. One category of improvements is pulse sequence design for faster acquisition of the same amount of data. Echo-planar methods acquire a whole plane of k-space in one or a few excitations [23]. These methods are sensitive to field inhomogeneities, chemical shift effects and signal decay during the long read-out. Gradient pulse optimization can be used to some extent to reduce the repetition time, but ultimately, gradient hardware or peripheral nerve stimulation caused by rapid gradient switching sets a limit. Another way of reducing acquisition times is to collect fewer points in k-space. By exploiting spatiotemporal structure of the object being imaged, essentially the same images can be reconstructed from less data. Scan time is reduced by a so-called reduction factor. One should bear in mind, though, that almost all of these acquisition time reduction techniques come at the cost of increased noise in the reconstructed image. Modelling of the signal using various kinds of priors, thereby fitting the actual data to the model, is commonly used. This model fit is obviously erroneous if the data does not conform to the model. The difficulty lies in finding good models, that can also be exploited in MRI. Below is a short list of common methods to shorten acquisition time.

Partial Fourier imaging

Traditional Fourier encoding consists of acquiring a Cartesian sampling of

k-space with sufficient sampling density to avoid spatial aliasing. A k-space is acquired that covers spatial frequencies high enough to encode the desired resolution. After a fast Fourier transform, a complex image is reconstructed. The image should ideally be real, which is equivalent to a Hermitian symmetry in k-space. Half of k-space could therefore be reconstructed from the other half, eliminating the need for acquiring a symmetric k-space. In practice, the image is not real, but some phase variations are present, mainly due to inhomogeneities in the magnetic field, caused by susceptibility effects. These phase variations usually vary slowly over the image. By acquiring slightly more than half of k-space (typically 55–65%), the phase variations can be reconstructed from the symmetric part of k-space and removed from the data [24]. The remaining image is then more or less real.

Non-Cartesian encoding

It is not necessary to acquire a Cartesian sampling of k-space. Other sampling schemes may be beneficial. Instead of acquiring a rectangular k-space, a circular one can be acquired, having the same spatial resolution in all directions. This eliminates the need to acquire the corners of k-space. Spiral read-out trajectories [25] instead of linear ones can cover larger parts k-space per repetition, and is sometimes referred to as echo-planar imaging methods. Radial and spiral sampling schemes also show more forgiving aliasing artifacts when using undersampling than Cartesian sampling. Non-Cartesian sampling will, however, require more complicated reconstruction. This typically involves a process called gridding [26], or a non-uniform Fourier transform [27].

HYPR

Projection imaging has gained much interest, because of the forgiving appearance when using large undersampling factors and thus rapid image acquisition. HighlY constrained backPRojection (HYPR) [28] has demonstrated an impressive reduction factor of 225 for time resolved imaging. Temporal averaging is used to reconstruct a composite image, which is then used to constrain backprojections of individual radial read-outs, depositing the projection data only in the objects being imaged. This requires, however, that the objects in the imaging volume do not change position over time. Thus, while it might be useful for contrast enhanced vessel angiography, it is not directly applicable for imaging of cardiac motion.

Parallel imaging

By exploiting the low-frequency spatial encoding and simultaneous signal reception of surface coils, parallel imaging methods, such as SENSitivity Encoding (SENSE) [29] or GeneRalized Autocalibrating Partially Parallel

Acquisition (GRAPPA) [30] can be used to decrease scan time. In these methods, k-space is undersampled, causing spatial alias overlap. This overlap can be recovered since there are several measurements by the individual coil elements, and the aliased signal components are encoded with different coil sensitivity. Acquisition may be shortened by a reduction factor up to the number of coils used in signal reception, but noise becomes an issue with high reduction factors. This is caused by signal and noise correlation between the coils; the coils essentially sees the same signal when using a large number of coils. Typical reduction factors when using SENSE are 2–3.

Keyhole, BRISK, TRICKS

Keyhole [31], Block Regional Interpolation Scheme for k-space (BRISK) [32] and Time-Resolved Imaging of Contrast Kinetics (TRICKS) [33] are techniques that use varying temporal sampling density for different parts in k-space. The central lines are typically acquired every time frame and the outer k-space lines are acquired more seldom, e.g. every second or third time frame. The idea is that the main part of the image contrast lies in the center of k-space. The signal model assumes that the dynamic information has low spatial frequency, which is not valid for moving edges but may be useful in contrast enhanced angiography.

Reduced field of view

Reduced field of view (RFOV) [34, 35] assumes that the field of view can be divided into a static region and a dynamic region. A fully sampled k-space can then be acquired for one time frame, while dynamic imaging can be limited to the smaller dynamic part of the field of view. Spatial aliasing overlap will occur in the dynamic data, but can be recovered because the static data is known.

UNFOLD

Unaliasing by Fourier-Encoding the Overlaps Using the Temporal Dimension (UNFOLD) [36] samples the k-t space in an interlaced fashion; odd k-space lines are sampled in odd time frames and even k-space lines in even time frames. If the time frames are reconstructed individually, spatial aliasing overlap will occur, due to the undersampling. The aliasing signal will, however, appear with alternating phase between the time frames and can be filtered out. This is, in principle, an extension of the model used in RFOV imaging. Instead of dividing the FOV in an entirely static and a fully dynamic region, some motion is allowed in the static region. The FOV is thus divided into a high dynamic region and a low dynamic region. If the regions are exactly one half of the FOV apart, the particular undersampling in k-t space can be seen as overlapping the low dynamic region with the high dynamic region, but with one of the regions shifted in temporal

frequency by one half of the temporal bandwidth. In this sense, the full temporal sampling bandwidth can be shared between the two regions. By extending the sampling bandwidth by as much bandwidth as is contained in the low dynamic region, both signals will fit without aliasing. The extra bandwidth needed is usually much less than the factor of 2 gained by the undersampling. UNFOLD can also be seen as a special case of *k-t* BLAST, described below.

***k-t* BLAST and *k-t* SENSE**

A method for dynamic imaging that has gained much attention over the last few years is *k-t* BLAST (Broad-use Linear Acquisition Speed-up Technique) [37]. One of the reasons for its popularity is the high achievable reduction factors. Two-dimensional and three-dimensional acquisitions with reduction factors of 5 or 8 have been presented with very high image quality. The principle of the method will be described in detail in Section 4.1. The *k-t* BLAST approach can also incorporate multiple coils and their spatial sensitivity to improve reconstruction. This is called *k-t* SENSE, which is more of a multiple-coil extension of *k-t* BLAST than a combination of *k-t* BLAST and SENSE.

4.1 *k-t* BLAST

4.1.1 The *x-f* space

As described in Section 3.3, when sampling the *k-t* space regularly, signal aliasing is introduced in the reciprocal *x-f* space. In typical cardiac imaging contexts, the signal content in *x-f* space has a very localized appearance. Many spatial positions have a very narrow temporal bandwidth. This is shown in Figure 4.1.

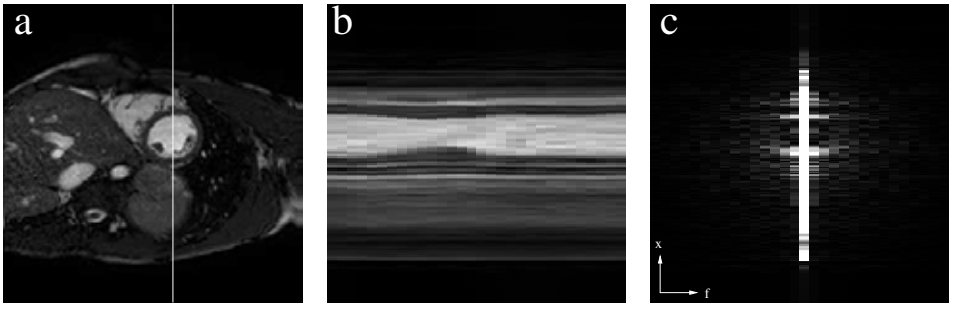

Figure 4.1: One time frame from a 2D cardiac acquisition (a), from which one column has been selected (white line). The column's development over time (b) has a signal distribution in *x-f* space that is very localized (c).

Because one can control the sampling of *k-t* space, one can also control how the aliased signals are packed in the *x-f* space. It is not necessary to sample the *k-t* space on an axis aligned grid. A sheared grid, forming a lattice, is still regular and will create periodic aliasing in the *x-f* space. The locations of the aliased signals will then also form a lattice. Using lattice sampling, the localized aliased signals can be packed tighter, enabling reduced sampling density in *k-t* space and thus faster acquisition. Two examples of *k-t* lattice sampling and the corresponding signal packing are shown in Figures 4.2.

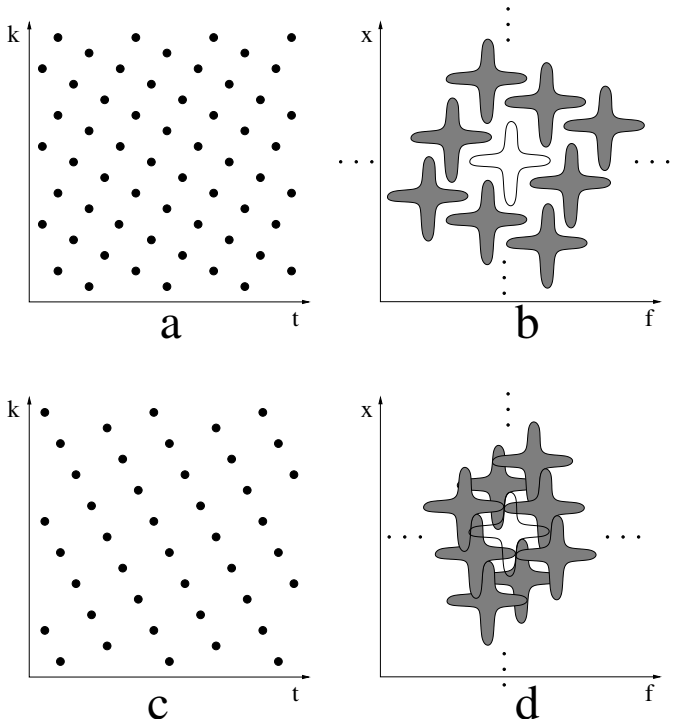

Figure 4.2: Dense sampling on a *k-t* lattice (a) and the corresponding signal packing in *x-f* space (b). Tight signal packing with no overlapping ensures alias free reconstruction. Too sparse lattice sampling in *k-t* space (c), on the other hand, packs signals too tight in *x-f* space, causing overlapping and thus prohibits correct reconstruction.

Essentially, UNFOLD uses this principle, because the interlaced sampling pattern used in UNFOLD is also a lattice. A fixed predetermined filter is then used to recover the signal. The filter is a temporal low-pass filter with different bandwidths for the high and low dynamic regions. The use of a fixed filter imposes a limit on the packing, because the bandwidth

of the filter in the whole high-dynamic region must be wide enough to capture the dynamics of the highest bandwidth in the region. The *k-t* BLAST approach uses a filter more closely matched to the actual data, enabling potentially tighter packing and thus higher reduction factors. Furthermore, this filter can be used to suppress signal where the aliased signals dominate over the main signal. This involves obtaining an estimate of the main signal distribution without aliasing. This estimate can be used to further improve upon UNFOLD by using a reconstruction filter adapted to the measured data.

4.1.2 Fast estimation of signal distribution in *x-f* space

Typical *x-f* signal distribution of cardiac objects have an additional property that can be exploited. The temporal bandwidth varies reasonably slowly over the spatial dimensions. Especially, regions with low temporal bandwidth usually form large continuous regions. An estimate of the signal distribution does not need to be of high spatial resolution [38], but only indicate where there is strong signal with high temporal bandwidth. The signal distribution estimate, sometimes referred to as training data, can thus be measured by sampling only the central lines in *k*-space. Because an alias-free estimate is desired, these lines have to be sampled with full temporal bandwidth, i.e. sampled in every time frame.

A schematic illustration of the *k-t* BLAST approach is shown in Figure 4.3. The *k-t* space is sampled using a sparse lattice, containing high resolution data with aliasing, and a dense region in the center of *k*-space in all time frames, containing information to estimate the signal distribution in *x-f* space. Since the sampling pattern is known, the positions of the aliased signals are also known. By knowing both an estimate of the true and the aliased signal distributions, one can suppress aliasing in the signal reconstruction.

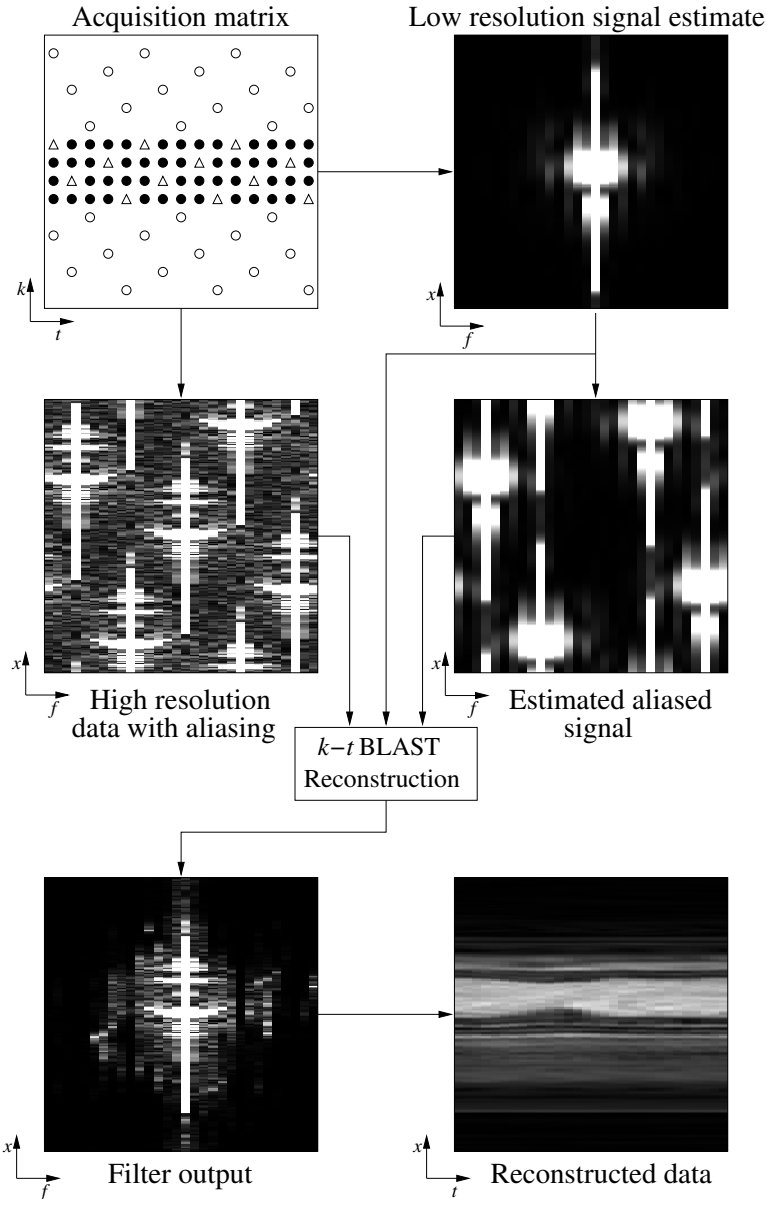

Figure 4.3: Schematic illustration of the *k-t* BLAST approach. The *k-t* space is sampled in two ways. Central lines in *k*-space (triangles and black circles) are fully sampled, yielding a low resolution estimate of the signal distribution. The sparse lattice (triangles and hollow circles) yields high resolution data with aliasing. An estimate of the aliased signal can be obtained from the signal estimate and sampling lattice. Through Wiener filtering, the aliasing can be suppressed, and a Fourier transform in time yields the final output. The data used in this figure is the same as in Figure 4.1.

4.1.3 The *k-t* BLAST reconstruction filter

The measured signal from the lattice sample points is a sum of the true signal and aliased signals, originating from other spatial locations and temporal frequencies. By treating the signal in each spatial position as wide-sense stationary in time, a Wiener filter approach can be used to filter out the aliased signal. Furthermore, measurement noise is also expected, so the Wiener filter becomes

$$\frac{M^2}{M^2 + \sum M_{alias}^2 + \Psi^2} \tag{4.1}$$

where M^2 is the signal distribution estimate, $\sum M_{alias}^2$ is the estimated aliased energy as shown in Figure 4.3 and Ψ^2 is the measurement noise variance.

The *k-t* BLAST reconstruction filter can be seen as a quotient between the the desired signal energy estimate and the measured signal energy estimate, consisting of the sum of the true signal, the aliased signal and the measurement noise. Summing the signals in this way is appropriate for uncorrelated signals. The aliased signal is from different spatial locations and temporal frequencies, by lattice design, and correlation is thus expected to be very low. The measurement noise is mainly caused by thermal noise emitted by the subject and in the receiver electronics. The noise is Gaussian white [39], as long as one considers the complex signal measured. The measurement noise variance can be obtained by measuring the variance for a homogeneous region in the image, such as the background. For reconstruction of a wide-sense stationary source with wide-sense stationary noise, the Wiener filter is the optimal linear estimator in the least squares sense [40].

The effect of the filter varies depending on the amount of signal overlap in *x-f* space. In areas with no overlap, the filter reduces to an ordinary noise suppressing Wiener filter, passing signal where it is dominant over the measurement noise. Where there is no true signal, the aliasing and noise is efficiently removed. Where there is overlap, the filter will favor the dominant signal, passing signal if true signal is dominant or blocking signal if aliasing or noise is dominant.

This filtering process is intuitively performed by multiplication in the *x-f* space, but a corresponding convolution filter kernel in *k-t* space can also be considered. Such a filter would fill in the blank positions in the *k-t* space which are not on the sampling lattice.

4.1.4 Implementation details

Lattice optimization

The locations of the aliased signals are determined by the sampling lattice in *k-t* space. Thus, different sampling lattices can cause differing amounts of signal overlap and different reconstruction performance. Maximizing the minimum distance between the signal aliases can be done independently of the object being imaged, and is only dependent on field of view, temporal resolution and reduction factor [41]. Maximizing minimum alias distance, however, does not guarantee minimum overlap. To minimize overlap, the actual signal distribution for the particular acquisition has to be taken into account, which is a much larger problem.

Reconstruction from arbitrary sampling in *k-t* space has been derived, but direct analytic solution to the problem was deemed infeasible due to computational complexity [37]. Iterative solution to this problem has been presented [42], enabling the use of non-Cartesian *k-t* BLAST. This may be valuable even when using Cartesian lattice sampling, because the sample points will deviate from the lattice due to cardiac or respiratory phase estimation errors.

Baseline subtraction

The temporal variation of the signal can be modeled as a deviation from a baseline signal. This baseline can be estimated by computing the temporal average of each *k*-space line. This baseline estimate is subtracted from both the signal distribution estimate and the lattice sampled data before filtering. The baseline is then added after the filtering step.

It is argued that treating this baseline separately will avoid reconstruction errors that can otherwise be introduced in the filtering [37]. The baseline signal does contain the by far strongest signal which could warrant special treatment since it can be estimated in this alternative way.

Filtering the signal distribution estimate

Since the signal distribution estimate is obtained by measuring very few lines in the central parts of *k*-space, and reconstructed by zero-filling the outer parts, ringing artifacts may occur. Therefore, some window, typically a Hamming window, is used to reduce this ringing, though the benefits are reported to be subtle [38].

The original *k-t* BLAST paper [37] proposes temporal low-pass filtering of the signal distribution estimate, to reduce noise with high temporal

frequencies. This will also have the effect of suppressing high frequency signals, effectively lowering achieved temporal resolution. Filtering the signal distribution estimate itself will also have the unwanted side-effect of underestimating the high temporal frequencies of the aliased signal. This can be avoided by performing the temporal low-pass filtering after applying the reconstruction filter.

Using signal distribution estimate twice

All points in k-t space not on the lattice are reconstructed from the lattice samples using the reconstruction filter in Eq 4.1. This includes the central k-space lines already acquired for the signal distribution estimate. Instead of using these reconstructed points, they can be substituted for the measured data, especially if the central k-space lines were acquired in an interleaved fashion during the acquisition of the lattice samples. The measured central k-space lines can also be used in the baseline estimation. This will remove any aliasing in the lower spatial frequencies of the baseline estimate.

Chapter 5

Tensor field visualization

Visualization of tensor fields, a three dimensional volume where each point is a tensor, is a difficult problem. The general concept of a tensor, a multilinear mapping, is often impractical to visualize. Thus, many approaches are specialized for a particular application. In the case of myocardial deformation, after eigen decomposition, three eigenvectors and corresponding eigenvalues are obtained. The eigenvectors of the strain rate tensors represent the principal directions of instantaneous rate of shortening or lengthening. The eigenvalues indicate the rate of lengthening (positive value) or shortening (negative value). The tensor still has six degrees of freedom, making it impossible to solely use color coding.

5.1 Glyph visualization

A common way to visualize a tensor is to use a glyph, a geometric object, that can describe the degrees of freedom of the tensor. Such a glyph can for instance consist of three arrows, representing the eigenvectors, scaled by their corresponding eigenvalues. Since the eigenvalues can be negative, this can be shown by the color of the arrow, or by making two arrows, pointing outward for positive eigenvalues or inward for negative eigenvalues, as in Figure 5.1a. A more intuitive way, especially in the application of deformation, is to visualize the tensor as an ellipsoid with the principal axes along the eigenvectors and the corresponding radii set to some basis raised to the power of the eigenvalue [43]. This would map negative eigenvalues to a radius between 0 and 1 and positive eigenvalues to a value larger than 1. The resulting ellipsoid would be the result of deforming a unit sphere with this strain rate for some period of time. A two-dimensional example is shown in Figure 5.1b.

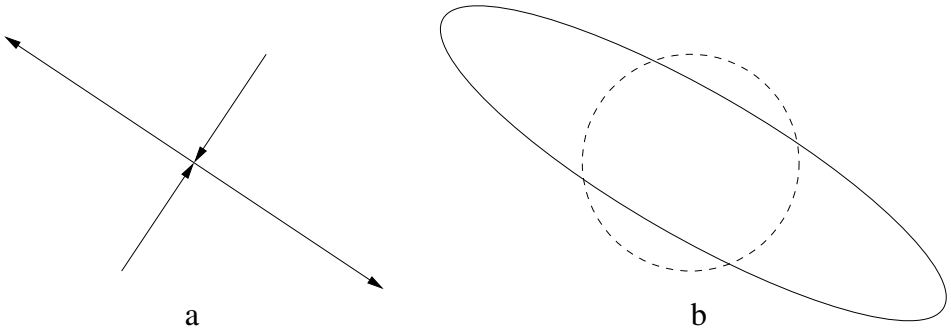

Figure 5.1: Glyph visualization of deformation. Arrow glyph representation showing eigenvectors and arrowheads indicate the sign of the eigenvalues (a). In the deformed circle visualization (b), the dashed unit circle represents an original state and the ellipse represents the shape of the circle after being deformed according to the deformation indicated with the arrows. For visualization of strain rate, the ellipse represents a circle after being affected by the strain rate for some period of time.

Using glyph rendering will allow description of all the degrees of freedom for a tensor. The approach is thus good for a single tensor, but becomes impractical for visualizing a whole field of tensors. Occlusion and visual cluttering makes this approach undesirable. The method suggested in Paper I is to separate visualization of a specific tensor of interest and the rest of the tensor field. The idea is to show all degrees of freedom for one tensor using glyph visualization, while some simplified global approach is used for the underlying tensor field. The tensor of interest can then be changed by navigating through the overview visualization.

5.2 Noise field filtering

A popular method in vector field visualization is Line Integral Convolution (LIC) [44]. It works by convolving a noise field along line integrals of the vector field. The convolution kernel is a smoothing kernel, typically a boxcar or Gaussian. The result, as illustrated in Figure 5.2, is a painting-like image with strokes along the vector field. The vector field is thus visualized using a scalar field, which basically contains structured white noise. The resolution of the scalar field typically needs to be higher than the resolution of the vector field, because structure with spatial extent is used to represent the vector value at a single point.

One of the advantages of LIC is that it preserves continuity of the vector field. The structures are connected along the vector field. LIC

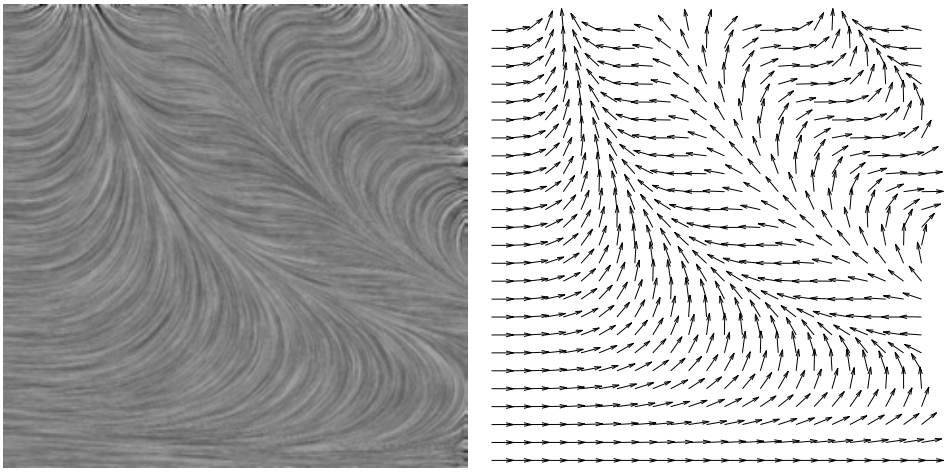

Figure 5.2: Two-dimensional LIC visualization for vector field visualization (a) of the vector field in (b). Note the continuous representation and lack of directionality in the LIC visualization.

has been adopted for tensor visualization by performing the convolution sequentially for the two dominant eigenvectors [45]. This is done with fixed convolution sizes, disregarding the degree of anisotropy, the relation between the eigenvalues, of the tensor field. The approach taken in Paper I is instead to keep the main idea of LIC, starting with a noise field and filter it according to the tensor field. The output is a *scalar* field, with structure representing the tensor field, that in the three dimensional case can be visualized using volume rendering. The difference with respect to LIC is that filtering is no longer performed along a line, but in a linear, planar or spherical fashion or somewhere in between, depending on the tensor field. Some kind of adaptive filtering is thus necessary.

5.2.1 Enhancement

A method that uses adaptive filtering controlled by a tensor field is image enhancement [46, 47]. It is used to perform anisotropic low-pass filtering of images, avoiding filtering across edges and thereby blurring the image. In the first step, the local structure of the image is estimated into a structure tensor with the use of quadrature filters. This structure tensor contains large eigenvalues in directions of strong edges. In two dimensions, a tensor with two large eigenvalues corresponds to a point-like structure in the image, a tensor with one large eigenvalue corresponds to an edge and a tensor

with two small eigenvalues corresponds to a homogeneous region with no structure. In the first case, no low-pass filtering will be performed. In the second case, anisotropic low-pass filtering will be performed along the edge (across the eigenvector direction). In the last case, isotropic low-pass filtering is performed. The method readily extends to higher dimensions.

The filtering is performed by steerable filters. Instead of constructing a new filter for each neighborhood, a set of filters is used, consisting of one isotropic low-pass filter and several directed high-pass filters, as shown in Figure 5.3. The image is filtered using all filters, and the resulting output is produced by weighting the filter responses individually at each point according to the structure tensor. If the low-pass filter is combined with a high-pass filter in some direction, the result is an all-pass filter in that direction and a low-pass filter in the other directions. The high-pass components are added in directions with large eigenvalues, to preserve edges along these directions.

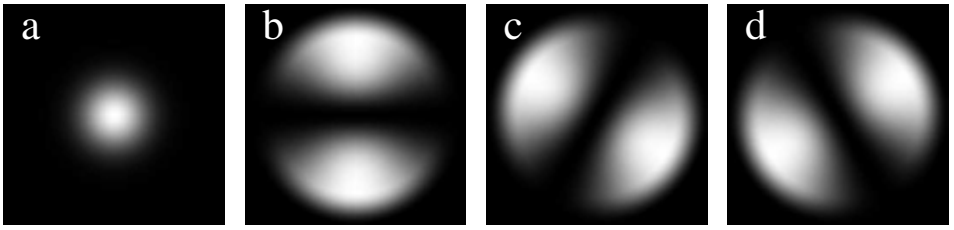

Figure 5.3: The filter set for two-dimensional steerable anisotropic filtering, consisting of one isotropic low-pass filter (a) and three directional high-pass filters (b-d). The filters can be combined linearly into an anisotropic low-pass filter of any direction.

The details of how the filter set is constructed and how the filter responses are combined are described in Paper I.

In the image enhancement method, a structure tensor is estimated from the image, and the structure tensor is then used to control the filtering by steering the filtering process. In the tensor visualization approach, the tensor field is already given. The image being filtered is an initial noise image. It is beneficial to iterate the filtering process in this case, in order to be able to create curved noise structures. In image enhancement, all-pass filtering is performed in directions of high eigenvalues and low-pass filtering is performed in directions of low eigenvalues. In visualization of strain rate tensors, the opposite is desired. This means low-pass filtering along strong eigenvalue directions, smearing the noise in these directions. The eigenvalues are therefore remapped to facilitate this. A further improvement of the method described in Paper I is to make use of the sign of the eigenvalue in

this mapping, similar to the mapping of eigenvalues to radii of the ellipsoid. The result is strong low-pass filtering along positive eigenvalue directions, medium low-pass filtering along zero eigenvalue directions and all-pass filtering along negative eigenvalue directions. In Figure 5.4, this is shown for a systolic and a diastolic cardiac phase using volume rendering. One-directional volume preserving expansion, implying contraction in the other two directions, is thus visualized as spike-like structure in the expansion direction. Correspondingly, volume preserving one-directional contraction is shown as disc-like structure. The resulting structure is thus reminiscent of the ellipsoid.

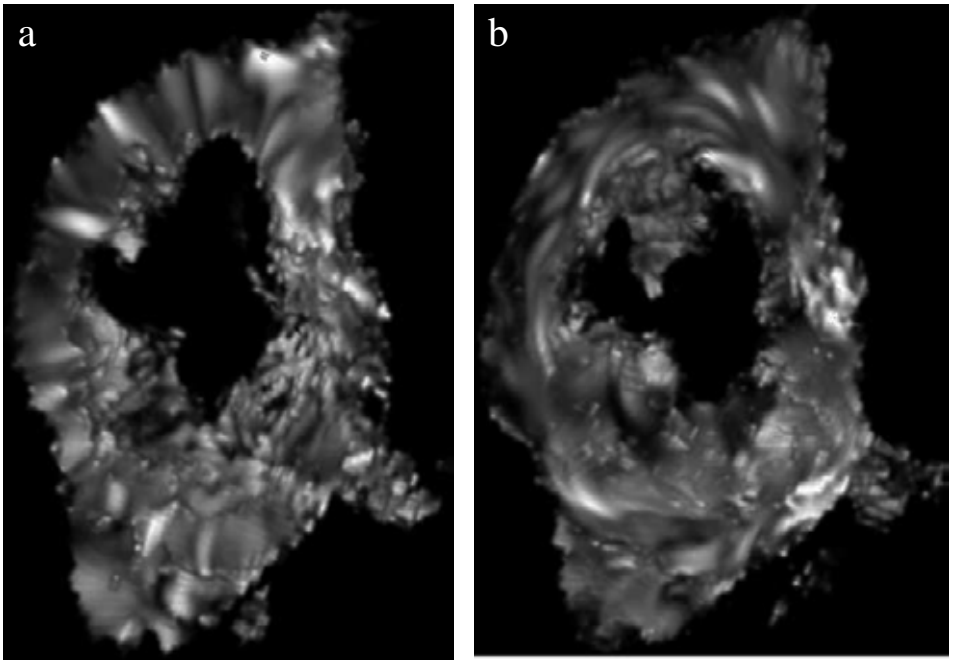

Figure 5.4: Tensor visualization of strain rate tensors in the heart wall of the left ventricle in a short-axis slab in systole (a) and diastole (b). The right-ventricle has been excluded for the purpose of clarity. In three dimensions, there is spike appearance in systole, depicting radial expansion, and onion layer appearance in diastole, depicting radial contraction.

This method can also been used to visualize other tensor fields. One example is diffusion tensor data representing fiber structure in the brain measured with MRI. In this case, there are no negative eigenvalues, easing eigenvalue remapping. Fiber tractography, a popular method for visualizing this type of data, creates a vector field out of the tensor data by explicit tracking [48], but runs into problems at locations of fiber crossings

where the vector model is inappropriate. An intrinsic tensor visualization approach handles this automatically. The method described in Paper I has successfully been applied on diffusion tensor data [49], and an output volume is shown in Figure 5.5.

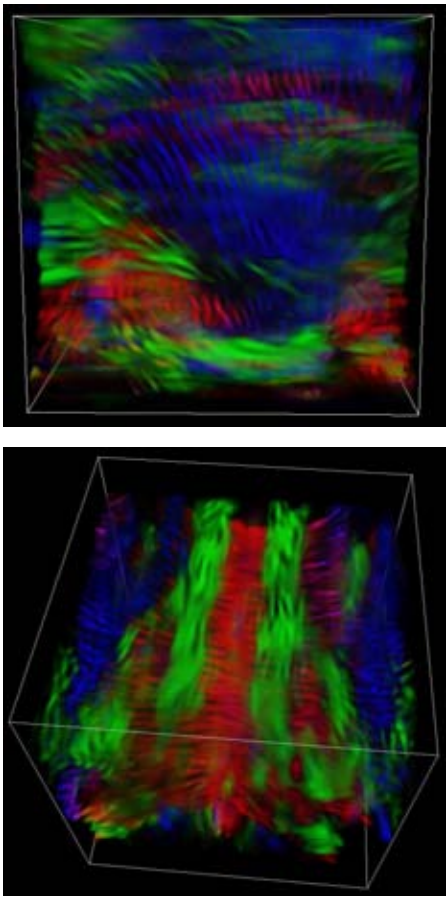

Figure 5.5: Volume visualization of fiber structure of the Corona Radiata in the human brain from two viewpoints. The volume is color coded according to the direction of the eigenvector corresponding to the largest eigenvalue (red = right–left, green = anterior–posterior, blue = superior–inferior). Corpus Callosum can be seen as the red structure. The green structures on top of Corpus Callosum (top figure) are the Superior Longitudinal Fasciculus. The motor-sensory fibers can be seen as the blue structure.

Chapter 6

Summary of papers

6.1 Paper I: Tensor Field Visualisation using Adaptive Filtering of Noise Fields combined with Glyph Rendering

This paper was presented at the IEEE Visualization conference in Boston 2002. The paper presents a method for tensor field visualization that integrates visualization of a tensor-of-interest with an overview visualization of the complete tensor field. The idea is to use glyph rendering to show the tensor-of-interest with all degrees of freedom, while avoiding cluttering and occlusion associated with glyph rendering of tensor fields. The rest of the tensor field is then visualized using an alternative approach. A cursor can be navigated through the background to change the location of the tensor-of-interest in real time. For the background visualization, a new method inspired by line integral convolution is presented. A scalar field is created from the tensor field with the use of tensor-controlled adaptive filtering. A noise volume is used as a seed input and then iteratively filtered, creating structure in the noise in the directions of strong eigenvalues of the tensor field.

6.2 Paper II: Five-dimensional MRI Incorporating Simultaneous Resolution of Cardiac and Respiratory Phases for Volumetric Imaging

This paper presents a novel method for volumetric MRI acquisition temporally resolved over both cardiac and respiratory cycles simultaneously. This creates a five-dimensional data set, opening new possibilities for studying

physiological effects caused by respiration on cardiac function. The method is based on an alternative gating approach extended to two temporal dimensions. The acquisition is controlled in real-time by continuously estimating cardiac and respiratory phase and sampling k-space individually for each time frame. The order of k-space traversal is optimized by using a Hilbert curve which minimizes jumps in k-space. This reduces eddy currents that cause artifacts when rapid pulse sequences are used.

6.3 Paper III: *k-t*^{2} BLAST: Exploiting Spatio-temporal Structure in Simultaneously Cardiac and Respiratory Time-resolved Volumetric Imaging

This paper presents an efficient way of sampling five-dimensional data. Data is commonly sampled regularly in k-t space, causing signal aliasing in the corresponding x-f space. By exploiting that the signal localized in x-f space, signals can be packed more densely. This translates to sparse lattice sampling in k-t space, reducing acquisition time. The sparse sampling results in signal aliasing in x-f space. This aliasing is suppressed by the use of a Wiener filter approach, which also suppresses noise. Using this method, an increase of spatial resolution by a factor of four is possible in half the scan time compared to full sampling in k-t space.

Chapter 7

Discussion

This thesis has presented new methods for imaging cardiac motion. Analysis and visualization of local deformation was accomplished by computing a strain rate tensor field from a velocity field measured by MRI and visualizing this tensor field using a combination of glyph rendering and overview visualization. The overview visualization was performed by volume rendering of a scalar field, computed by adaptive filtering of a noise field to create spatial structure. A method for volumetric imaging resolved over both the cardiac and respiratory cycles simultaneously was presented, enabling the study of interventricular coupling and septum shape in three dimensions, throughout the respiratory cycle. Acquisition efficiency was increased eight-fold by bandwidth sharing in x-f space, i.e. by packing the aliased signals tighter in x-f space.

7.1 Multidimensional imaging

This thesis presents imaging methods for high dimensional data. Myocardial deformation was represented as a tensor field with six degrees of freedom in every point in a time-resolved volume. This corresponds to an inner dimension of six and an outer dimension of four. Imaging of anatomical structures in the five-dimensional approach, resolving the cardiac and respiratory cycles in a volumetric acquisition, has an outer dimension of five. In Papers II and III, only scalar image data were acquired, i.e. having an inner dimensionality of one.

Routine clinical work as of today, on the other hand, often use traditional methods in lower dimensions. Echocardiography measures ultrasound reflectance or a one-directional Doppler shift in each sample point, corresponding to an inner dimension of one. This is performed along

one spatial line over time in M-mode echocardiography. Two-dimensional echocardiography extends this with one additional outer spatial dimension. There is no question that imaging in higher dimensions is more difficult and time-consuming, and thus more expensive. One may ask oneself what the extra dimensions add to what is used in clinical practice today. When it comes to physiological understanding, especially of the more complex interactions such as interventricular coupling or local myocardial deformation, directions and variations of motion is not known beforehand. Measuring motion in only one direction imposes assumptions of the data, which in the hand of a skillful operator might be quite reasonable for some applications. For research purposes, however, objectivity is important, and the goal is to reduce sensitivity to operator dependent acquisition, slice positioning, slice misregistration and angular error in velocity measurements. MRI studies have stressed the need of a three-dimensional characterization of the shape and curvature of the septum [50]. More comprehensive physiological understanding can lead to better assumptions regarding motion directionality and slice orientation sensitivity. This can then be transfered into lower dimensional methods, and to clinical routine.

7.2 Using *k*-t^2 BLAST for respiratory gating

$k-t^2$ BLAST may be used as an alternative to respiratory gating. Instead of acquiring data only in the end expiration period of the respiratory cycle, data can be acquired continuously, resolving the respiratory cycle. This will commonly require longer scan times, due to the fact that the end expiration period usually accounts for about half the respiratory cycle, while resolving the respiratory cycle to any desirable extent will require more than two respiratory time frames. This increase in scan time can avoided if $k-t^2$ BLAST is used for scan time reduction. One may then after reconstruction select just one respiratory time frame to simulate a respiratory gated acquisition. An advantage is that this removes the necessity of prior knowledge of the optimal respiratory phase.

7.3 Costs of sparse sampling

The reduction of acquisition time in *k*-*t* BLAST comes from sampling the *k*-*t* space less densely. There are definitively drawbacks of the sparse sampling of data, such as increased noise and reduced temporal fidelity.

7.3.1 Noise

It is in the nature of MRI that a shorter acquisition time means more noise. One may visualize this as foldover of noise, that the signal in *x-f* space is not really limited to the localized signal bearing parts, but there is a wideband noise component as well. If there are fewer sampling points in *k-t* space, more noise will fold over the desired signal. The massive reduction factors typically used in *k-t* BLAST means that very few data points are acquired. This will have effects on noise. In the application of cardiac imaging, this extra noise is usually accepted in order to reduce imaging times or increase resolution. Since voxel sizes in typical cardiac examinations are quite large, there is quite a lot of signal to begin with. Also, *k-t* BLAST carries an implicit Wiener filtering reducing the noise temporally. Nevertheless, spatial filtering and especially spatiotemporal filtering, along the lines of image enhancement [46, 47], might prove useful to reduce noise when high spatial resolutions are approached. In the case of five-dimensional imaging, edges have a lot of structure that can be exploited in noise reduction.

7.3.2 Temporal fidelity

The aim of the *k-t* BLAST method is to reduce imaging times *without* sacrificing image quality. When the signals in *x-f* space overlap, which is difficult to avoid, some reconstruction error is unavoidable. The use of the Wiener filter minimizes this reconstruction error in the least squares sense, but there is still a reconstruction error. Overlapping mostly occurs between high temporal frequencies of one spatial position and low temporal frequencies of a different spatial position. The reconstruction error is most prominent in high temporal frequencies. This is because the signal energy in the lower temporal frequencies is much stronger than in the high temporal frequencies and the optimal linear reconstruction from such overlap is to attenuate the least dominant signal. The result of this is a lower effective temporal bandwidth, i.e. temporal blurring.

This mechanism of alias overlap attenuation, suppressing the high temporal frequencies to retain the lower frequency content, will provide static images from *k-t* BLAST of very high quality. The aliasing which would arise if zero-filling reconstruction was performed will be minimized. The loss of temporal bandwidth is only fully exposed in the temporal dimension, and since this dimension is omitted in static images, a false impression of retained fidelity is presented. It is therefore important to study the temporal dimension when using *k-t* BLAST. This can either be done with the use

of animation or by using M-mode type visualization, where the temporal dimension is presented spatially.

The loss of temporal bandwidth is not equal to sampling with a lower frequency. Sometimes, high temporal bandwidth is used to suppress motion artifacts, not to resolve a particular temporal event. The temporal blurring caused by *k-t* BLAST is done by filtering out the high frequency content, not letting it alias onto the lower frequencies. In this case, the loss of effective temporal bandwidth is not a loss of relevant image information.

With the use of short-TR pulse sequences, such as balanced SSFP, it is possible to trade scan time for improved temporal resolution. By further applying *k-t* BLAST, the original scan time can be restored. In this way, the original temporal bandwidth should at least be preserved, but hopefully increased, because the bandwidth will be shared between different spatial positions. With a reduction factor of N, N different spatial positions will share an N-fold bandwidth. If some spatial positions have low bandwidth, which is very common in cardiac imaging, more sampling bandwidth is available to the other positions. What remains to be studied is the practical gain achievable and the cost of acquiring the signal distribution estimate and its effect on the accuracy of the Wiener reconstruction filter.

With two temporal dimensions, several parts of the *k-t* BLAST approach can be controlled to act differently in each dimension. One may, for instance, adjust lattice optimization in order to preserve temporal fidelity in one temporal dimension at the cost of increasing temporal blurring in the other dimension. Some applications desire high cardiac phase fidelity, but might accept a larger imaging window in the respiratory cycle, if *k-t*^{2} BLAST is used as a respiratory artifact reduction method. Other applications desire high respiratory phase fidelity, but can accept temporal blurring in cardiac phase dimension if the imaging is concentrated on the slow-varying diastolic cardiac phases.

7.4 Future work

7.4.1 Validation

The methods presented here need to be tested on more subjects and validated against other methods. One difficulty with validating the five-dimensional approach is that no other method produces similar data. Robustness and reproducibility can be tested more easily, though, since it only involves testing a method against itself.

7.4.2 Tensor field data quality

The estimation of the strain rate tensor involves computing differentials, which in practice often is implemented by finite differencing. This means that the process is highly sensitive to noise and image artifacts. The impact of noise and artifacts on the scalar representation of the tensor field used for background visualization has not been studied. Nevertheless, the visualization results are likely to benefit from improvements in data acquisition, especially regarding noise and respiratory motion artifacts.

7.4.3 Optimizing reduction factor versus temporal fidelity

When using k-t^2 BLAST, the effect of temporal blurring needs to be studied. A large reduction factor is favorable for reducing scan time or increasing spatiotemporal resolution, but also increases risk of loosing important temporal information. The appropriate reduction factor needs to be optimized for the individual applications. This is tightly coupled with the validation of the method.

7.4.4 Acquisition of velocity data using k-t^2 BLAST

Two-dimensional phase contrast MRI measurements resolving both cardiac and respiratory cycles has been presented previously [18] and shows promise of measuring important respiratory variations in blood flow. To this date, volumetric velocity acquisition resolved over both cardiac and respiratory cycles has not been performed. Five-dimensional acquisition in the form presented in Paper II is too time consuming to add velocity measurements. Acquisition time shortening, along the lines of k-t^2 BLAST presented in Paper III, is a prerequisite for five-dimensional velocity measurements. Not only will these measurements be free of respiratory motion artifacts, as described in Section 7.2, but it will also enable the studies of different flow patterns in different phases of the respiratory cycle. The right ventricle has highly respiratory dependent flow, and it's complex shape is best described using a volumetric acquisition.

7.5 Potential impact

The tensor field visualization presented in Paper I may help investigators in the study of local myocardial deformation using fully three-dimensional measurements. This may in turn be used to obtain new information as to

which directions and locations of deformations are important for diagnosis or follow-up of certain diseases and treatments.

Volumetric imaging resolving both cardiac and respiratory cycles simultaneously offers a completely new type of data. Study or quantification of shape and ventricular volumes over the course of the respiratory cycle may offer new means for physiological description of interventricular coupling. The method presented in Paper II for measuring such a data set has the potential to describe these phenomena.

Possibility to shorten acquisition time or increase resolution in cardiac imaging is always desired. The method presented in Paper III offers a way to not only use temporal correlation in the cardiac cycle, but also in the combined two-dimensional space of cardiac and respiratory cycles. This has the potential of reducing reconstruction error or allowing larger reduction factors. This is not only applicable in reducing imaging time and increasing spatial resolution for volumetric imaging, but may also be applied to single slice imaging for a far broader range of applications.

The *k-t* BLAST methods yield significant increase in imaging efficiency. There is no question that there is additional spatiotemporal structure inherent to the dynamics of cardiac and respiratory motion. Finding new ways to exploit these properties can open new possibilities and applications for cardiac MRI.

Bibliography

[1] Causes of Death 2003. Swedish National Board of Health and Welfare (Socialstyrelsen), Epidemiologiskt Centrum, 2005. http://www.socialstyrelsen.se/.

[2] Hatle L, Sutherland GR. Regional myocardial function — a new approach. Eur Heart J 2000;21(16):1337–1357.

[3] Guth BD, Schulz R, Heusch G. Time course and mechanisms of contractile dysfunction during acute myocardial ischemia. Circulation 1993;87:35–42.

[4] Weber KT, Janicki JS, Shroff S, Fishman AP. Contractile mechanics and interaction of the right and left ventricles. Am J Cardiol 1981; 47(3):686–695.

[5] Santamore WP, Dell'Italia LJ. Ventricular interdependence: Significant left ventricular contribution to right ventricular systolic function. Prog Cardiovasc Dis 1998;40(4):289–308.

[6] Wranne B, Pinto FJ, Siegel LC, Miller DC, Schnittger I. Abnormal postoperative interventricular motion: new intraoperative transesophageal echocardiographic evidence supports a novel hypothesis. Am Heart J 1993;126(1):161–167.

[7] Waggoner AD, Shah AA, Schuessler JS, Crawford ES, Nelson JG, Miller RR, Quinones MA. Effect of cardiac surgery on ventricular septal motion: assessment by intraoperative echocardiography and cross-sectional two-dimensional echocardiography. Am Heart J 1982; 104(6):1271–1278.

[8] Lehmann KG, Lee FA, McKenzie WB, Barash PG, Prokop EK, Durkin MA, Ezekowitz MD. Onset of altered interventricular septal motion during cardiac surgery. assessment by continuous intraoperative transesophageal echocardiography. Circulation 1990;82(4):1325–1334.

[9] Spencer AJM. Continuum Mechanics. Dover Publications, Inc., 1980.

[10] Axel L, Dougherty L. MR imaging of motion with spatial modulation of magnetization. Radiology 1989;171:841–845.

[11] Kvitting JPE, Sigfridsson A, Wigström L, Bolger AF, Karlsson M. Virtual makers for noninvasive assessment of myocardial dynamics. In 54th Annual Meeting of the Scandinavian Association for Thoracic Surgery. Bergen, Norway, 2005; 150.

[12] Pelc NJ, Herfkens RJ, Shimakawa A, Enzmann DR. Phase contrast cine magnetic resonance imaging. Magn Reson Q 1991;7(4):229–254.

[13] Kvitting JPE, Ebbers T, Engvall J, Sutherland GR, Wranne B, Wigström L. Three-directional myocardial motion assessed using 3D phase contrast MRI. J Cardiovasc Magn Reson 2004;6(3):627–636.

[14] Bracewell R. The Fourier Transform and its Applications. McGraw-Hill, 2nd edition, 1986.

[15] Lanzer P, Barta C, Botvinick EH, Wiesendanger HU, Modin G, Higgins CB. ECG-synchronized cardiac MR imaging: method and evaluation. Radiology 1985;155(3):681–686.

[16] Glover GH, Pelc NJ. A rapid-gated cine MRI technique. Magn Reson Annual 1988;299–333.

[17] Fredrickson JO, Pelc NJ. Time-resolved MR imaging by automatic data segmentation. J Magn Reson Imaging 1994;4(2):189–196.

[18] Fredrickson JO, Wegmuller H, Herfkens RJ, Pelc NJ. Simultaneous temporal resolution of cardiac and respiratory motion in MR imaging. Radiology 1995;195(1):169–175.

[19] Scheffler K, Lehnhardt S. Principles and applications of balanced SSFP techniques. Eur Radiol 2003;13:2409–2418.

[20] Jung BA, Henning J, Scheffler K. Single-breathhold 3D-TrueFISP cine cardiac imaging. Magn Reson Med 2002;48:921–925.

[21] Markl M, Leupold J, Hennig J. Double average parallel imaging for optimized eddy current compensation and steady state storage in balanced SSFP imaging. In Proceedings of ISMRM. Miami Beach, 2005; 503.

[22] Gotsman C, Lindenbaum M. On the metric properties of discrete space-filling curves. IEEE Transactions on Image Processing 1996; 5(5):794–797.

[23] McKinnon GC. Ultrafast interleaved gradient-echo-planar imaging on a standard scanner. Magn Reson Med 1993;30:609–616.

[24] Noll DC, Nishimura DG, Macovski A. Homodyne detection in magnetic resonance imaging. IEEE Trans Med Imag 1991;10(2):154–163.

[25] Nayak KS, Pauly JM, Yang PC, Hu BS, Meyer CH, , Nishimura DG. Real-time interactive coronary MRA. Magn Reson Med 2001;46:430–435.

[26] O'Sullivan JD. A fast sinc function gridding algorithm for Fourier inversion in computer tomography. IEEE Trans Med Imaging 1985; MI-4(4):200–207.

[27] Dutt A, Rokhlin V. Fast Fourier transforms for nonequispaced data. SIAM J Sci Comput 1993;14(6):1368–1393.

[28] Mistretta CA, Wieben O, Velikina J, Block W, Perry J, Wu Y, Johnson K, Wu Y. Highly constrained backprojection for time-resolved MRI. Magn Reson Med 2006;55:30–40.

[29] Pruessman KP, Weiger M, Scheidegger MB, Boesiger P. SENSE: sensitivity encoding for fast MRI. Magn Reson Med 1999;42:952–962.

[30] Griswold MA, Jakob PM, Heidemann RM, Nittka M, Jellus V, Wang J, Kiefer B, Haase A. Generalized autocalibrating partially parallel acquisitions (GRAPPA). Magn Reson Med 2002;47:1202–1210.

[31] van Vaals JJ, Brummer ME, Dixon WT, Tuithof HH, Engels H, Nelson RC, Gerety BM, Chezmar JL, den Boer JA. "Keyhole" method for accelerating imaging of contrast agent uptake. J Magn Reson Imaging 1993;3(4):671–675.

[32] Doyle M, Walsh EG, Blackwell GG, Pohost GM. Block regional interpolation scheme for k-space (BRISK): a rapid cardiac imaging technique. Magn Reson Med 1995;33:163–170.

[33] Korosec FR, Frayne R, Grist TM, Mistretta CA. Time-resolved contrast-enhanced 3D MR angiography. Magn Reson Med 1996; 36:345–351.

[34] Hu X, Parrish T. Reduction of field of view for dynamic imaging. Magn Reson Med 1994;31:691–694.

[35] Madore B, Fredrickson JO, Alley MT, , Pelc NJ. A reduced field-of-view method to increase temporal resolution or reduce scan time in cine MRI. Magn Reson Med 2000;43:549–558.

[36] Madore B, Glover GH, Pelc NJ. Unaliasing by fourier-encoding the overlaps using the temporal dimension (UNFOLD), applied to cardiac imaging and fMRI. Magn Reson Med 1999;42:813–828.

[37] Tsao J, Boesiger P, Pruessman KP. k-t BLAST and k-t SENSE: Dynamic MRI with high frame rate exploiting spatiotemporal correlations. Magn Reson Med 2003;50:1031–1042.

[38] Hansen MS, Kozerke S, Pruessmann KP, Boesiger P, Pedersen EM, Tsao J. On the influence of training data quality in $k-t$ BLAST reconstruction. Magn Reson Med 2004;52:1175–1183.

[39] Sijbers J, den Dekker AJ, Audekerke JV, Verhoye M, Dyck DV. Estimation of the noise in magnitude MR images. Magnetic Resonance Imaging 1998;16(1):87–90.

[40] Mallat S. A Wavelet Tour of Signal Processing. Academic Press, 1999.

[41] Tsao J, Kozerke S, Boesiger P, Pruessmann KP. Optimizing spatiotemporal sampling for $k-t$ BLAST and $k-t$ SENSE: Application to high-resolution real-time cardiac steady-state free precession. Magn Reson Med 2005;53:1372–1382.

[42] Hansen MS, Baltes C, Tsao J, Kozerke S, Pruessmann KP, Eggers H. $k-t$ BLAST reconstruction from non-cartesian $k-t$ space sampling. Magn Reson Med 2006;55:85–91.

[43] Kirby RM, Marmanis H, Laidlaw DH. Visualizing Multivalued Data from 2D Incompressible Flows Using Concepts from Painting. In D Ebert, M Gross, B Hamann, eds., IEEE Visualization '99. San Francisco, 1999; 333–340.

[44] Cabral B, Leedom LC. Imaging Vector Fields Using Line Integral Convolution. Computer Graphics 1993;27(Annual Conference Series):263–270.

[45] Hsu E. Generalized Line Integral Convolution Rendering of Diffusion Tensor Fields. In Proceedings of the International Society for Magnetic Resonance in Medicine, 9th Scientific Meeting and Exhibition, Glasgow, UK. 2001; 790.

[46] Knutsson H, Wilson R, Granlund GH. Anisotropic non-stationary image estimation and its applications — Part I: Restoration of noisy images. IEEE Transactions on Communications 1983;31(3):388–397.

[47] Granlund GH, Knutsson H. Signal Processing for Computer Vision. Kluwer Academic Publishers, 1995. ISBN 0-7923-9530-1.

[48] Basser PJ, Pajevic S, Pierpaoli C, Duda J, , Aldroubi A. In vivo fiber tractography using DT-MRI data. Magn Reson Med 2000;44:625–632.

[49] Sigfridsson A, Estepar R, Wigström L, Alberola C, Westin CF. Diffusion tensor visualization using random field correlation and volume rendering. In Proc. of th 9th International Workshop on Computer Aided Systems Theory. Las Palmas de Gran Canaria (Spain): Universidad de Las Palmas de Gran Canaria, 2003; 41–45.

[50] Moses DA, Axel L. Quantification of the curvature and shape of the interventricular septum. Magn Reson Med 2004;52:154–163.